ELSEVIER

Ultramicroscopy 83 (2000) 129–139

ultramicroscopy

www.elsevier.nl/locate/ultramic

Charging phenomena in PEEM imaging and spectroscopy

B. Gilbert[a,*], R. Andres[b], P. Perfetti[d], G. Margaritondo[a], G. Rempfer[d], Gelsomina De Stasio[c,e]

[a]*Institut de Physique Appliquée, Ecole Polytechnique Fédérale, PH-Ecublens, CH-1015 Lausanne, Switzerland*
[b]*Paul Scherrer Institut, CH 5232 Villigen PSI, Switzerland*
[c]*Istituto di Struttura della Materia del CNR, Via Fosso del Cavaliere, 00137 Roma, Italy*
[d]*Department of Physics, Portland State University, P.O. Box 751, Portland, OR, USA*
[e]*UW – Madison Physics Department, 1150 University Avenue, Madison, WI 53706-1390, USA*

Received 3 August 1999; received in revised form 5 November 1999

Abstract

Spectromicroscopy with the imaging technique of X-ray photoelectron emission microscopy (X-PEEM) is a microchemical analytical tool installed in many synchrotron radiation laboratories, and which is finding application in diverse fields of research. The method of sample analysis, X-ray absorption spectroscopy, does not encounter the same problems as X-ray photoemission spectroscopy when sample charging occurs, hence even good insulators may often be analyzed without any apparent artifacts in images or spectra. We show, however, that charging effects cannot be neglected. We model the effect of surface charge formation on the secondary electron yield from uniform samples to demonstrate that surface charge primarily reduces the yield of electrons which may contribute to the detected signal. We illustrate that on non-uniform insulating samples, localized centers of charge may substantially affect microscope imaging and resolution as the electrostatic field close to the surface is distorted. Finally, in certain circumstances non-uniform surface charge may lead to unexpected lineshapes in X-ray absorption spectra causing, in some extreme cases, negative spectra. These negative spectra are explained, and several strategies are reviewed to minimize the impact of sample charging when analyzing poorly conducting samples of any nature.

PACS: 61.10.H; 78.70.D; 61.16.M; 87.64

Keywords: XANES; X-ray absorption spectroscopy; Photoelectron microscopy; Chemical analysis in biophysics; Photoelectron imaging; XANES spectroscopy; Spectromicroscopy; Charging

1. Introduction

High-resolution imaging of samples can be performed using electrostatic lenses that capture electrons reflected from or emitted by a surface. Low-energy electron microscopy (LEEM) [1] and photoelectron emission microscopy with UV light (UV-PEEM) [2] are laboratory-based devices that reach below 10 nm lateral resolution. As well as observing topography, image-contrast derives from local variations in low-energy electron reflectivity for the first technique and in work function for the second. X-ray illumination from a synchrotron source can be monochromatized and continuously varied in energy, which allows a related instrument,

* Corresponding author.

0304-3991/00/$ - see front matter
PII: S0304-3991(99)00196-5

the X-PEEM to additionally acquire chemical information [3]. The specimen is studied by X-ray absorption near edge structure (XANES) spectroscopy by measuring the total electron yield as a function of photon energy, with a lateral resolution reaching 20 nm. X-PEEM images may then contain additional contrast, depending on photon energy, due to X-ray absorption by localized elements in a specific chemical state.

A number of such X-PEEMs are operational at synchrotron light sources worldwide [4–7]. The MEPHISTO spectromicroscope [8], installed at the Synchrotron Radiation Center of the UW-Madison, is depicted in Fig. 1. Experimentally, X-PEEM has proven to be extremely flexible for the study of a wide range of materials, the greatest constraint on the sample properties being ultra high vacuum compatibility. Examples of specimens studied include magnetic storage devices [9], tribological surfaces [10], cell cultures and tissue sections [11,12]. Current reviews of X-ray microscopy and spectromicroscopy demonstrate an even wider range of application [13,14].

As with all methods of analysis using electrons as probes of a sample surface, the study of poorly conducting samples may cause surface charging. Many reviews describe charging effects in XPS, which can cause the measured core level binding energies to shift (to lower energies) by up to several hundred eV [15]. The effect is much less severe (and often undetectable) for absorption measurements, however, as although the yield of secondary electrons may be lowered, the assumption that it is proportional to the actual absorption coefficient is still rather good.

Instruments which perform XANES spectroscopy in the microscopic domain are more susceptible to artifacts due to charging, especially if there is severe localized charging. The trajectories of the emitted secondary electrons contain the spatial information of the sample surface, but charged areas distort these trajectories, with consequences for both imaging and spectroscopy. As a greater variety of samples are analyzed in this kind of imaging X-PEEM microscopes there will be more opportunity for charging phenomena to affect data acquisition. We present a description of charging induced artifacts with examples and review strategies to avoid them.

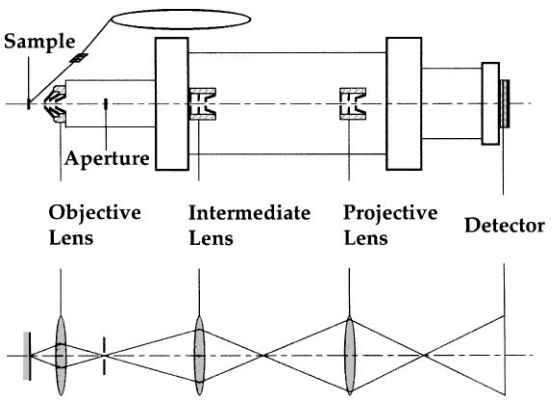

Fig. 1. Scheme of the MEPHISTO X-PEEM. Monochromatized X-rays from a synchrotron source excite photoemission from the sample surface. The photoelectrons are accelerated into the electron optics and a magnified image is formed on a detector (chevron style multichannel plate and phosphor screen). The microscopic aperture in the back focal plane of the objective lens aids spatial resolution by rejecting all but a narrow band of photoelectron kinetic energies (corresponding to low-energy secondary electrons in the sample) and hence reducing chromatic aberration.

2. Description of uniform charging in total yield spectroscopy

The signal detected in total yield XANES spectroscopy is the low-energy tail of the photoelectron energy distribution curve [16]. At a core level absorption edge, a proportion of the high-energy Auger electrons emitted by the absorbing atom scatter inelastically within the sample to produce a distribution of low-energy electrons that is rather independent of photon energy or sample characteristics. The depth inside the sample from which the emitted electrons originate is characterized by the mean free path (MFP) length for free electrons in the material. The MFP is greater for low-energy (secondary) electrons than for high-energy electrons (primary and Auger electrons) and greater also for insulating materials than metals. In most cases, the electron MFP is much smaller than the photon penetration depth, and we make this assumption in the subsequent analysis.

The yield of secondary electrons (per unit area) from a surface illuminated by a photon flux I_o can generally be expressed as

$$Y(h\nu) = \pi I_o M(h\nu) \int_{\phi}^{\infty} P(E)\,\mathrm{d}E. \quad (1)$$

In Eq. (1) $M(h\nu) \propto h\nu\rho\mu(h\nu)$; where $\mu(h\nu)$ is the X-ray mass attenuation coefficient, ρ the density and $h\nu$ the photon energy [5]. $M(h\nu)$ represents the absorption of energy within a surface layer of depth $\delta < \Delta$, where Δ is the $1/e$ photon attenuation length, and δ is the effective X-PEEM sampling depth. $P(E)$ describes the energy distribution function of secondary electrons incident upon the solid-vacuum interface. Only the proportion of electrons with enough energy to escape the work function surface potential, Φ, actually leave the sample, and hence the range of integration begins at Φ. $P(E)$ depends upon the nature of the medium through the low-energy electron MFP. The MFP is dependent upon the properties of the medium, more specifically the extent of electron – electron and electron – phonon scattering for metallic, semiconductor or insulating materials.

In an imaging technique the X-ray beam is not tightly focused, so typically the field of view is smaller than the illuminated sample area. For a uniform conducting sample, the photocurrent is balanced by conduction electrons from the sample holder. If the sample is an insulator, the formation of a surface layer of positive charge reduces the yield until at equilibrium the photocurrent is once more balanced by conduction through the sample thickness and by surface conductivity. The formation of positive charge reduces the yield in two ways. Recombination events, as electrons travel to the surface, reduce the number of electrons incident at the solid–vacuum interface, and at the surface there is a higher potential barrier due to the surface voltage V_s (which can be considered as a contribution to a higher effective work function, $\Phi_{\mathrm{eff}} = \Phi + V_s$). Neglecting recombination loss and surface conductance, the sample can be modeled as a photoemitting surface taking current from ground through a capacitance and resistance in parallel. Balancing the current in the circuit gives

$$j = eAY = i_C + i_R, \quad (2)$$

where j is the photocurrent, A the illuminated area, i_C and i_R are the currents through the capacitance and resistance, respectively, and the yield Y varies due to charging as given in Eq. (1) with the lower limit of integration replaced by $\Phi_{\mathrm{eff}} = \Phi + V_s$.

Henke et al. have performed the integration of Eq. (1) to find the secondary electron yields for metallic, semi-conducting or insulating samples [17,18]. In the case of insulating samples the yield is inversely proportional to the work function. To illustrate the effects of sample charging we modify their result by replacing the work function with an effective work function, which gives for the photocurrent

$$j = \frac{\beta}{\Phi + V_s} \text{ where } \beta = \frac{eAI_o M(h\nu) f(\lambda)}{4 \sin \varphi}. \quad (3)$$

All terms in Eq. (3) are defined as earlier, except for $f(\lambda)$ which describes the primary and secondary scattering lengths in the medium. Eq. (2) can now be written in terms of j and solved to obtain implicitly the evolution of the photocurrent, $j(t)$, after an X-ray beam strikes an insulating sample. At time $t = 0$, $V_s = 0$, hence $j_o = \beta/\phi$.

$$j = \frac{-C\beta}{j^2}\frac{\mathrm{d}j}{\mathrm{d}t} + \frac{1}{R}\left(\frac{\beta}{j} - \Phi\right) \quad (4)$$

giving

$$\mathrm{e}^{-t/RC} = \left(\frac{j}{j_o}\right)^{\beta/ab}\left(\frac{j-a}{j_o-a}\right)^{-\beta/a(b-a)}\left(\frac{j-b}{j_o-b}\right)^{\beta/b(b-a)}, \quad (5)$$

where R and C are the sample bulk resistance and surface capacitance, respectively, and $a = j_+, b = j_-$ are the roots of the quadratic in j obtained when factorizing (4): $j_\pm = -\phi/2R \pm \frac{1}{2}\sqrt{(\Phi^2 + 4\beta R)}$. Eq. (5) is valid for $[j_{(t=0)} = j_o] \geqslant j > [j_{(t=\infty)} = a]$, where a is the positive root and the asymptotic limit of j at large t, that is, the equilibrium value of j. The neglect of surface charging and recombination are significant simplifications, but the resulting picture has the correct behavior, as seen in Fig. 2.

The dynamics of charging are shown experimentally by Fig. 2, which follows the evolution with time of the photocurrent from homogeneous conducting or insulating samples illuminated with

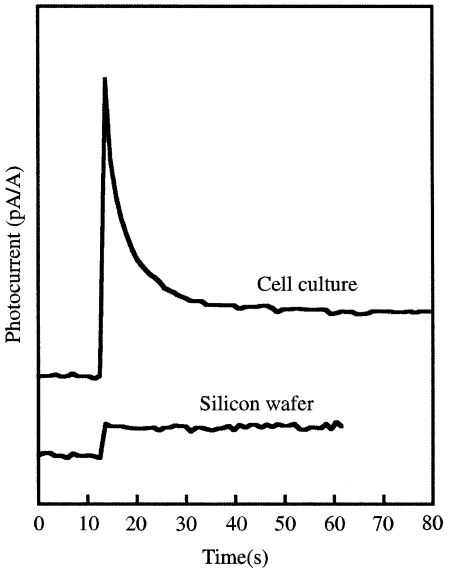

Fig. 2. Typical photocurrent versus time curves for insulating (a fixed human glioblastoma cell culture) and conducting (silicon wafer) samples illuminated with 538 eV X-ray photons (at the O 1s edge). A picoammeter connected between the sample mounting and ground measures the total emitted current after the illumination began (at approximately 14 s). The curves are normalized to the synchrotron beam current and displaced vertically for clarity. As explained in the text, charge formation at the surface of the cell culture reduces the yield of emitted electrons with time.

538 eV X-rays. The simple yield curve for the silicon wafer is stable, while charge build-up on the insulating cell sample causes an exponential-like reduction in photocurrent with time. Although the equilibrium yield is evidently significantly lower for the cell sample than the peak (initial) yield, the XANES spectra acquired on this sample have no spurious features or energy shifts due to the charging behavior. At equilibrium the yield remains proportional to the absorption cross section through the factor $M(h\nu)$ in Eq. (1). In general on homogeneous samples, charging effects, if extreme, may mean that total yield absorption spectroscopy is impossible, but if a signal is obtained at equilibrium, as in Fig. 2, then it contains the XANES information without artifacts. The case of spectra acquisition with spatial resolution, however, may occasionally suffer from artifacts of localized charging as described below.

3. Imaging effects of localized charging

While the formation of a uniform charging layer may reduce the total photoelectron yield, localized charging due to lateral inhomogeneities may additionally cause image artifacts by deviating the trajectory of emitted electrons. The imaging of electrons with electrostatic lenses is sensitive to any situation (usually sample topography) for which emitted electrons are not parallel to the optical axis. Localized charging can also make electron trajectories non-coaxial, and hence generate apparent topography. A typical example is an insulating feature on a conducting surface: electrons emitted by the feature, *and* from nearby regions of the conducting material are deflected by the charging spot. This lensing effect results in a dark halo around the object (strongly deviated electrons from nearby areas do not pass the aperture in the back focal plane of the objective lens) which is itself imaged out of focus. Such lensing effects give a strong but incorrect visual impression of surface relief. The situation is depicted schematically in Fig. 3a.

The study of insulating films on steel for applications in tribology and wear research provided many examples of charging features. With heat and rubbing, the monophosphate engine oil additive ZDDP forms highly resilient polyphosphate films, which are also good electrical insulators [10]. Film formation is uneven, resulting in islands that charge

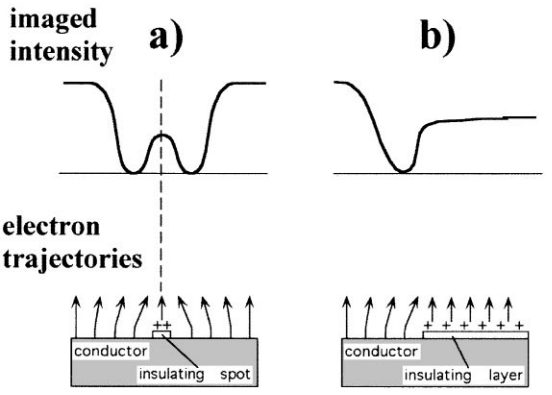

Fig. 3. Schematic illustrations of the effect of localized charge areas on the trajectories of emitted electrons, and on the subsequent intensity distribution at the electron detector, for (a) a charged spot and (b) a charged layer.

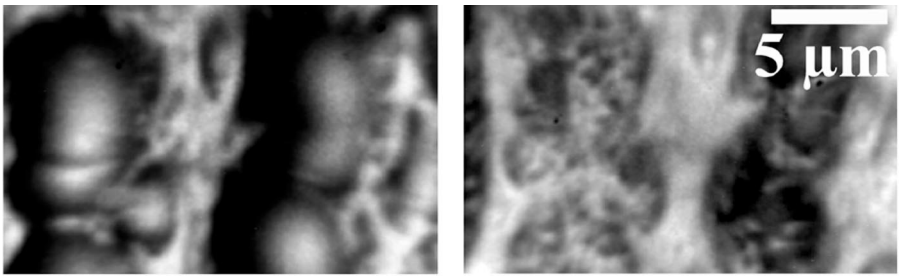

Fig. 4. MEPHISTO micrographs of a region of insulating polyphosphate film created on steel by the motor oil additive ZDDP. Both images are of the same specimen surface area, with a photon energy 140 eV (P 2s edge), but at different times. The initial image (a) exhibits extreme charging behavior. After 2 h of continuous illumination, much more sample detail is visible in (b) The change is attributed to permanent photon-induced surface modification which caused an increase in surface conductivity.

under X-ray illumination, as shown in Fig. 4a. The appearance of the films in MEPHISTO evolved with time. Fig. 4b was taken on the identical sample region as Fig. 4a but after 2 h of continuous illumination. Fig. 4b shows the modified appearance in the photoelectron image, with less artificial (charging induced) topography, and with more structural detail visible. We interpret the changes as being due to irreversible film damage due to X-ray exposure, resulting in increased electrical conductivity. The characteristically smooth forms imaged in Fig. 4b indicate that although the conductivity has increased, charging still occurs to a lesser degree.

The MEPHISTO spectromicroscope frequently analyses biological samples (cell cultures, tissue sections) which are poor conductors, but photoemit when sufficiently thin and mounted on a conducting gold substrate. Tissue mounted in epoxy and ultramicrotomed can be imaged for section thicknesses of 30–500 nm. Fixed tissue sections or cell cultures, 3–10 μm in thickness exhibit substantial charging unless first ashed and consequently thinned in an oxidative UV/ozone environment to remove carbon [19].

Even ashed samples can show charging induced artificial topography, as demonstrated in Fig. 5. Additionally, Fig. 5 shows how the sample appearance may vary with photon energy as this crosses an absorption threshold. The main feature in Fig. 5 is a gap in ashed human meningioma tissue which reveals the underlying gold substrate. Each pair of images (a and b, c and d) shows the photoelectron images, respectively, below and above the calcium 2p and oxygen 1s absorption edges. Calcium and oxygen spectra, acquired from a uniform tissue area are shown for reference. The ashed tissue charges under the beam, while the mostly empty gold substrate region remains neutral. At the substrate–tissue border, electrons photoemitted from the gold substrate are deviated from a coaxial trajectory and cannot pass through the aperture: hence, the corresponding image area appears dark. The situation is depicted schematically in Fig. 3b. As the extent to which the trajectories are perturbed varies smoothly away from the border, the effect in the image is of a smooth, three-dimensional protruding feature, which is only an artifact, as Fig. 5c makes clear.

The total yield varies substantially above and below the oxygen 1s edge at 538 eV, with the corresponding difference in the extent of charging above and below the edge. The calcium 2p edge at 349 eV lies closer to lower-energy edges of other physiologically present elements (potassium, carbon, sulfur, phosphorus) and hence there is a much smaller difference in the on- and pre-edge images.

A comparison of Fig. 5c and d shows that the effect of charge-induced apparent topography may vary strongly with photon energy. This effect is shown most vividly when the individual photoelectron micrographs, taken at incremental photon energies, are stacked together and animated to form a movie. The images of Fig. 5 were extracted from such movies, which can be found on-line at http://www.src.wisc.edu/mephisto/mephisto_movies.htm The movies clearly demonstrate another effect of sample charging: image defocusing with photon energy. The charge at the surface of an insulating sample affects the image formation

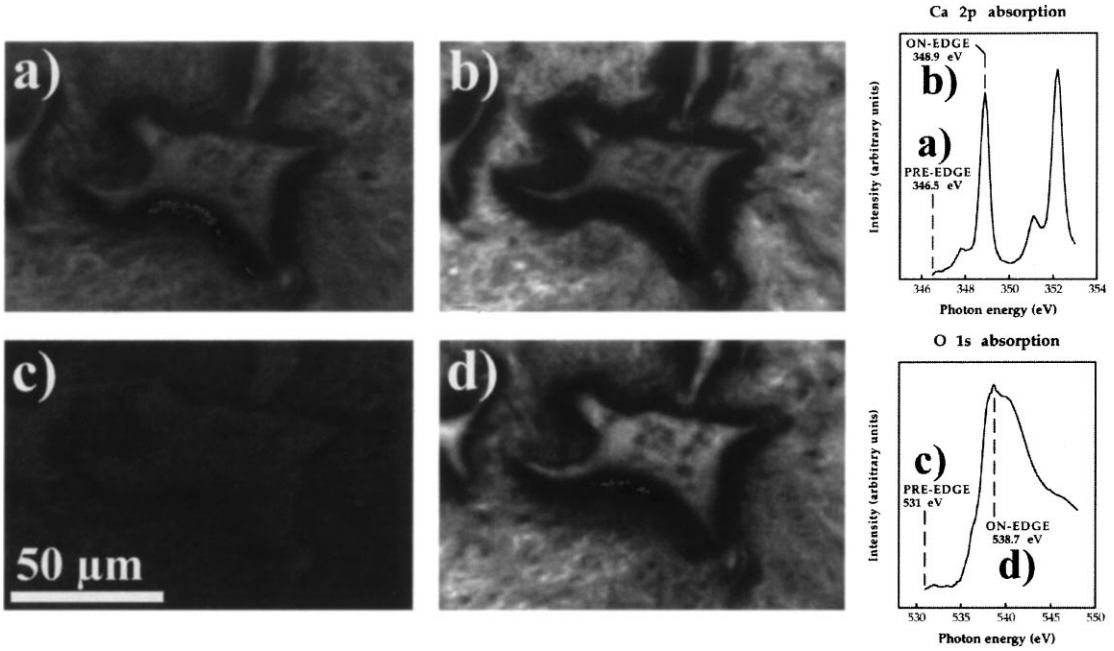

Fig. 5. MEPHISTO micrographs of ashed human meningioma tissue on silicon. The central feature is a gap in the tissue which reveals the underlying substrate. These images show charging induced apparent topography, which varies in degree with the photon energy. Micrographs (a) and (b) are below and above the calcium 2p edge, at 346.5 and 348.9 eV, respectively. The Ca 2p spectrum is displayed on the right. Micrographs (c) and (d) are below and above the oxygen 1s edge, at 531 and 538.7 eV, respectively. The O 1s spectrum is also displayed on the right. As explained in the text, the extent of surface charging can vary across absorption edges. Micrograph (c), just below the oxygen edge gives the flattest and most accurate image of the sample, with no artificial topography.

through the optics by changing the potential difference between the sample surface and the grounded first element of the objective lens. This accelerating potential is exactly the variable used to focus the photoelectron image on the detector (note that in an X-PEEM the focus voltage also affects the magnification). The movie across the oxygen 1s edge, which exhibits the largest charging effect, shows that both the magnification and the focus move with the photon energy. The effect is smaller at the calcium edge, but the movie explicitly shows two defocusing events which coincide with the two 2p peaks.

4. Spectroscopic effects of localized charging

An unexpected phenomenon, which is explained by considering the dependence of localized charging on photon energy, was the acquisition of negative XANES spectra from the specimen of Fig. 5 and others. The physical situation that may create this is described as follows. Consider a localized feature which is less conductive than the surrounding specimen. As the energy of the incident photons crosses an absorption threshold of that element, localized charging will cause the electrical potential to drift more than the surrounding specimen. When such a feature charges, the trajectories of electrons emitted from nearby are deflected, and are less likely to pass through the optics aperture. As the extent of charging varies dynamically with the photon energy, spectra from nearby regions will contain energy-dependent intensity losses, which are greatest close to the charging feature. Here, the fluctuations may pull the intensity below even the background (pre-edge) level, creating negative dips in the total yield spectra, which perfectly follow the spectrum of the feature itself.

Fig. 6 shows the positive and negative calcium 2p spectra acquired from the tissue–substrate border

regions shown with arrows in Fig. 5d. Spectra from within both tissue and substrate areas are positive, while negative spectra are observed at the border.

5. Strategies to minimize charging effects

The spectra of Fig. 6 clearly show that localized charging may affect the line shape of total yield spectra from samples that appear to be sufficiently conductive to allow the extraction of electrons. More generally, severe charging can make impossible X-PEEM analysis of many classes of specimens that would be of interest, for example thick biological samples (cells) or insulating materials science specimens (polymers, composite materials).

Two simple approaches of eliminating charging effects (false topography and negative spectra) were tested on the tissue sample of Fig. 5. By lowering the photon flux on the sample, the reduced rate of electron extraction will reduce the overall surface charging once the equilibrium is reached. The series of images in Fig. 7 show a detail of the tissue–substrate border of Fig. 5, and the effect of drastically reducing photon flux. This was achieved by specially reducing the stored beam current of the Aladdin synchrotron from 150 mA, to 10 and to 1 mA. A noticeable reduction of apparent topography is evident along the series – the width of the black band around the substrate is reduced – but at a large cost in image brightness and quality. Both the brightness and contrast of the last two images had to be digitally enhanced after data acquisition so that the features were clearly visible.

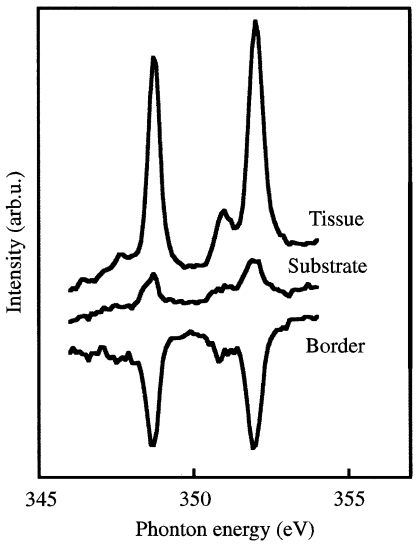

Fig. 6. Calcium 2p X-ray absorption spectra from tissue, substrate and border regions of the specimen imaged in Fig. 5. Normal positive 2p peaks are acquired from the substrate (conducting) and the ashed tissue (poorly conducting), but negative spectra are acquired from the substrate – tissue border. Note that the Ca 2p spectrum from the substrate is weak as calcium in this sample originates from cells, and there is much less in intracellular spaces.

The accompanying spectra were taken from the region marked with a box in the first image. All spectra have been treated and normalized identically, and are plotted on the same scale. Although the second spectrum is slightly less negative than the first, the very low photon flux meant that spectroscopy was almost impossible in the final case.

The series of images in Fig. 8 show the effect of increasing the diameter of the electron optics back focal aperture. As described earlier, the effect of deflecting the trajectories of electrons reduces their transmission through the system, so increasing aperture size allows a greater solid angle of electron trajectories to pass. Fig. 8 shows that by passing from 20 μm to 50 and 150 μm apertures more of the initially dark border region is successively imaged. The accompanying spectra from the region marked by a box were again treated identically, and are plotted on the same scale. They show that initially negative spectra become positive at large aperture diameter. It can be seen in these images, however, that the image resolution is worse with larger apertures.

The data presented in Figs. 7 and 8 confirm the interpretation of negative spectra as being due to the effects of localized charging on electron trajectories. However, the use of low flux, or large aperture to minimize the effect are not viable because of the disadvantages of each approach. A method used in XPS is to flood a charging sample with low-energy electrons to neutralize surface charge. This is impractical in the present experimental configuration as the sample is held at over -10 kV to accelerate the emitted electrons towards the optics. Similar charging problems have been encountered by Habliston et al. in the UV imaging of biological

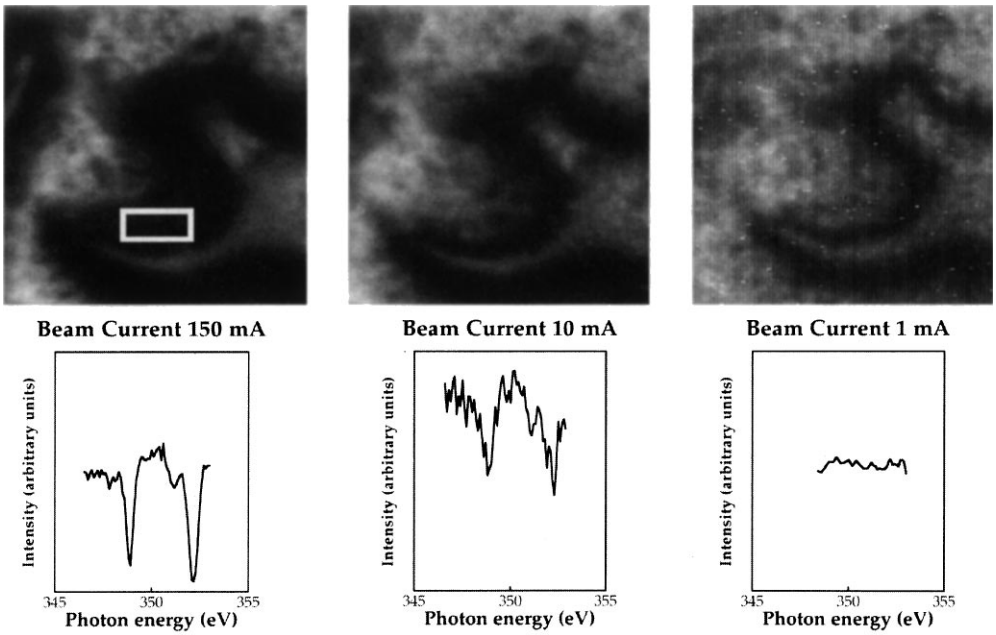

Fig. 7. The effect of X-ray illumination intensity on charging artifacts. The series of micrographs show the variation in appearance of a detail of the specimen shown in Fig. 5 as the incident intensity is reduced. The photon energy in each case is 538 eV, and the synchrotron beam current (a measure of X-ray intensity) decreases from left to right, having the values 150, 10 and 1 mA. The dark substrate – tissue border evident in the first image becomes relatively brighter at lower intensity, indicating less severe surface charging. The overall image intensity is much reduced, however, and the last two images have been digitally enhanced. The corresponding series of Ca 2p spectra were from the area shown by the white rectangle in the first image. There is no substantial elimination in the negative spectrum intensity, and the signal is too weak in the final case.

specimens in a PEM which operates on the same principles as MEPHISTO, although without the capability to do spectroscopy [20,21]. Since the main contrast mechanisms in this approach are (i) topographical and (ii) work function differences, the evaporation of cesium onto the surface of fixed cells enhanced the emitted yield and reduced charging, since alkali metals have very low work functions. A second technique was to simultaneously illuminate the sample with UV light, at high-energy ($h\nu > \Phi$, the work function) to stimulate the emission of secondary electrons for imaging and with visible light ($h\nu < \Phi$) to induce photoconductivity by internal photoemission. Very striking results were obtained in which an insulating cell body that was completely dark due to charging under only 254 nm illumination initially was imaged bright when photoconductivity was stimulated by 325 nm light from an HeCd laser.

A similar experiment was performed in MEPHISTO. We aimed to simultaneously illuminate a typical insulating biological sample with X-ray photons and photons from a mercury lamp lower in energy than the work function. A high-pressure mercury lamp was installed outside a sapphire window of the MEPHISTO main chamber with a fused quartz lens to approximately focus the light onto the sample in front of the objective lens. The UV light was transmitted through filters which block photons higher in energy than the filter cut-off energy.

Fig. 9 contains a sequence of plots of photocurrent versus time that demonstrate some success in alleviating surface charging by concurrent UV and X-ray illumination. We measured the photocurrent emitted by the sample due to X-ray light and saw an increase when the UV source was uncovered. The specimen was a culture of fixed human glioblastoma

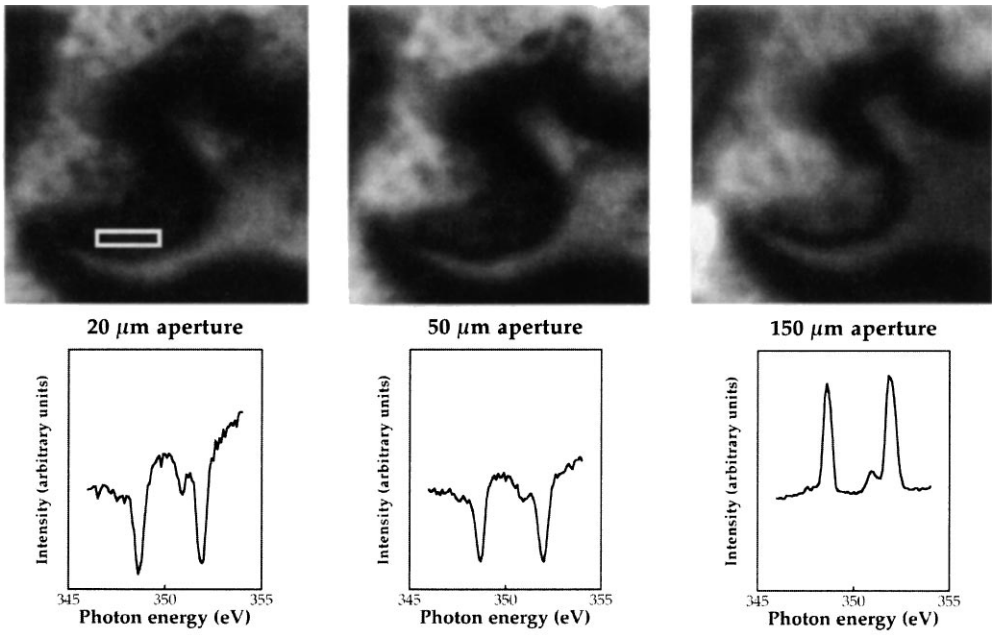

Fig. 8. The effect of electron optics aperture size on charging artifacts. The series of micrographs show the variation in specimen appearance as successively larger diameter apertures are placed in the objective lens back focal plane. The photon energy in each case is 538 eV, and the aperture diameters are 20, 50 and 150 μm. With larger apertures, more electrons, including those deflected from the optical axis by surface charge, are passed through the optics. Although image resolution is degraded, negative spectra are eliminated and the substrate – tissue border is brightened.

cells on a gold substrate which was impossible to image in MEPHISTO because of extreme charging. As it is not possible to measure the current of secondary electrons transmitted through the electron optics of MEPHISTO, the photocurrent was measured on a picoammeter connected between the sample mounting and ground. The plots show the typical reduction in yield after initial exposure to X-rays as surface charge builds up. The specimen was then exposed to filtered UV light, using 305, 320 or 335 nm cut-off filters. Then the X-ray beam was shuttered off, so that the specimen was only exposed to filtered UV light. Finally, the UV lamp was also shuttered off.

In each case, adding UV illumination to X-ray illumination causes a higher photocurrent. In all but the final curve, this is due to both increased surface conductivity, as well as photoemission by the filtered UV light. The final curve, taken with the 335 nm filter, shows that there is no photoemission caused by light less than 3.8 eV in energy (the photocurrent goes to zero when only UV light illuminates the sample). The increase in X-ray-stimulated photocurrent in the presence of UV illumination can then solely be attributed to an increase in surface conductivity due to surface-internal photoemission, which allows surface charge to be neutralized. In each case, the increase in yield is not instantaneous but gradual. The rate of increase is governed by the rate at which newly promoted conduction electrons can travel from outside of the X-ray spot to neutralize the charge inside, forming a dynamic equilibrium in which surface photocurrent flows radially into the X-ray-illuminated area from the (larger) UV-illuminated area.

The increase in yield detected in the presence of UV light did not allow a noticeable improvement in MEPHISTO imaging. For imaging in MEPHISTO a potential of approximately -12 kV is applied between the sample and the first element of the

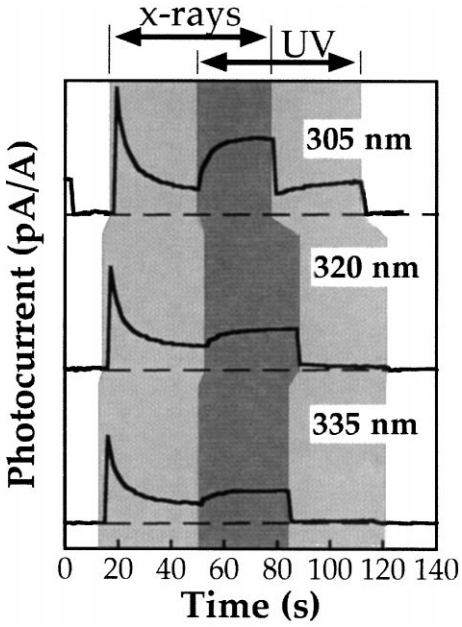

Fig. 9. Photocurrent curves for the simultaneous illumination of a fixed culture of human glioblastoma cells by 538 eV X-rays and by light from a filtered UV lamp, using low pass cut-off filters at the wavelengths indicated. Under X-ray light alone, the photocurrent follows the exponential-like decay from the initial value, which is typical of a charging sample. In each case, when the UV lamp shutter is removed the photocurrent increases. For filter cut-off wavelengths of 305 and 320 nm, the increase is partly due to additional photoemission stimulated by UV photons, shown by the finite photocurrent that is measured when the X-rays are stopped but the filtered UV illumination remains. An increase in surface photoconductivity due to internal photoemission also increases the yield by reducing surface charging. With the 335 nm cut-off filter, no photocurrent is observed with filtered UV-light alone, hence the increase in photocurrent is due to photoconductivity alone.

objective lens, which is ground, while no such bias was applied when the photocurrent was measured through a picoammeter. The decay in photocurrent in the presence of this accelerating potential immediately after X-ray illumination was observed to be much faster than when no bias is applied. This suggests that the electric field effectively removes all emitted electrons and reduces the probability that low-energy electrons may recombine with the positively charged surface. After rapidly reaching equilibrium, filtered UV illumination photoconductivity did not increase the surface conductivity enough to improve image brightness. A greater flux of visible photons is therefore required to sufficiently induce photoconductivity and improve MEPHISTO image brightness on such insulating samples.

6. Conclusions

Sample charging in XANES spectroscopy is generally less detrimental to the analysis of poorly conducting samples than for the related technique of XPS. A uniform insulating sample under X-ray illumination experiences the formation of a surface layer of positive charge that reduces the photocurrent until equilibrium is attained. Although the photocurrent is lower due to charging, if the signal level allows the acquisition of total yield XANES spectra then they accurately show the X-ray absorption fine structure. When XANES spectroscopy is combined with X-PEEM imaging and microchemical analysis, however, localized charging of insulating regions may dramatically affect the imaging and spectroscopy of nearby areas. The most extreme example is the acquisition of negative absorption peaks from a specimen area close to a strongly charging region. Charging centers deflect the trajectories of electrons emitted from nearby areas, and if the extent of charging varies across absorption edges there may be energy-dependent intensity fluctuations recorded in spectra from the surrounding sample area.

The situation more frequently encountered is that X-PEEM analysis is completely impossible if a sample is a very good insulator. Preparing the sample very thinly (less than 100 nm) may improve conduction across the bulk. Alternatively, studying the sample in a transmission geometry [22,23] separates the absorption of photons (which is independent of charging) for chemical analysis, from the emission of photoelectrons (from a metal photocathode) for imaging and spectroscopy. Not all samples can be prepared for transmission experiments, and in some cases the surface chemistry, rather than the bulk information is the subject of study. If such a sample cannot be studied because of charging, then only an increase in the surface conductivity offers a solution. This may be achieved by evaporating a metallic surface onto the sample, or by inducing photoconductivity. Photoconduction

elimination of charging has been demonstrated for the UV-PEEM, and shown here to be feasible. Future work to obtain a higher density of visible light photons incident upon the charging surface is expected to allow MEPHISTO imaging of insulating biological samples.

Acknowledgements

Work supported by the Fonds National Suisse de la Recherche Scientifique, the Consiglio Nazionale delle Ricerche and the Ecole Polytechnique Fédérale of Lausanne. The ZDDP sample was provided by G. Canning and G.M. Bancroft. Human cell and tissue samples were provided by R. Pallini, A. Rinelli and L.M. Larocca, and the cultures were prepared by P. Casalbore and Delio Mercanti. We benefited from the professional assistance of Mark Bissen and all the staff of the SRC (a national facility supported by the NSF under grant DMR-95-31009). We also thank Roger Hansen for use of the UV/ozone cleaning oven for the ashing of tissue samples.

References

[1] E. Bauer, Sur. Sci. Lett. 5 (1998) 1275.
[2] O.H. Griffith, W. Engel (Eds.), Proceedings of the Second International Symposium and Workshop on Emission Microscopy and Related Techniques (special issue), Ultramicroscopy 36 (1990).
[3] B.P. Tonner, G.R. Harp, Rev. Sci. Instrum. 5 (1988) 853.
[4] Ch. Ziethen, O. Schmidt, G.H. Fletcher, C.M. Schneider, G. Schonhense, R. Fromter, M. Seider, K. Grzelakowski, M. Merkel, D. Funnemann, W. Swiech, H. Gundlach, J. Kirschner, J. Elec. Spectrosc. Rel. Phenom. 88–91 (1998) 983.
[5] R. Wichtendahl, R. Fink, H. Kuhlenbeck, D. Preikszas, H. Rose, R. Spehr, P. Hartel, W. Engel, R. Schlogl, H.-J. Freund, A.M. Bradshaw, G. Lilienkamp, Th. Schmidt, E. Bauer, G. Benner, E. Umbach, Surf. Rev. Lett. 5 (1998) 1249.
[6] Th. Schmidt, S. Heun, J. Slezak, J. Diaz, K.C. Prince, G. Lilienkamp, E. Bauer, Surf. Rev. Lett. 5 (1998) 1287.
[7] S. Anders, H.A. Padmore, R.M. Duarte, T. Renner, T. Stammler, A. Scholl, M.R. Scheinfein, J. Stohr, L. Seve, Boris Sinkovic, Rev. Sci. Instrum. 70 (1999) 3973.
[8] Gelsomina De Stasio, M. Capozi, G.F. Lorusso, P.A. Baudat, T.C. Droubay, P. Perfetti, G. Margaritondo, B.P. Tonner, Rev. Sci. Instrum. 69 (1998) 2062.
[9] M. Mundschau, J. Romanowicz, J.Y. Wang, D.L. Sun, H.C. Chen, Surf. Rev. Lett. 5 (1998) 1269.
[10] G.W. Canning, M.L. Suominen Fuller, G.M. Bancroft, M. Kasrai, J.N. Cutler, G. De Stasio, B. Gilbert, Tribology Lett. 6 (1999) 159.
[11] G. De Stasio, D. Mercanti, M.T. Ciotti, T.C. Droubay, P. Perfetti, G. Margaritondo, B.P. Tonner, J. Phys. D 29 (1996) 259.
[12] B. Gilbert, J. Redondo, P.-A. Baudat, G.F. Lorusso, R. Andres, E.G. Van Meir, M.-F. Hamou, T. Suda, D. Mercanti, M.T. Ciotti, T.C. Droubay, B.P. Tonner, P. Perfetti, G. Margaritondo, Gelsomina De Stasio, J. Phys. D 31 (1998) 2642.
[13] H. Ade (Ed.), Special Issue J. Electron Spectrosc. Rel. Phenom. 84 (1997).
[14] J. Thieme, G. Schmahl, D. Rudolph, E. Umbach (Eds.), Microscopy and Spectromicroscopy, Springer, Heidelberg, 1998.
[15] S. Gunther, A. Kolmakov, J. Kovac, M. Kiskinova, Ultramicroscopy 75 (1998) 35.
[16] J. Stohr, NEXAFS Spectroscopy, Springer Series in Surface Sciences, Vol. 25, Springer, Heidelberg, 1992.
[17] B.L. Henke, J.A. Smith, D.T. Attwood, J. Appl. Phys. 48 (1977) 1852.
[18] B.L. Henke, J. Leisegang, S.D. Smith, Phys. Rev. B 19 (1979) 3004.
[19] Gelsomina De Stasio, B. Gilbert, L. Perfetti, R. Hansen, D. Mercanti, M.T. Ciotti, R. Andres, V.E. White, P. Perfetti, G. Margaritondo, Anal. Biochem. 266 (2) (1999) 174.
[20] D.L. Habliston, K.K. Hedberg, G.B. Birrel, G.F. Rempfer, O.H. Griffith, Biophys. J. 69 (1995) 1615.
[21] G.F. Rempfer, K.K. Nadakavukaren, O.H. Griffith, Ultramicroscopy 5 (1980) 437.
[22] Gelsomina De Stasio, B. Gilbert, Luca Perfetti, T. Nelson, M. Capozi, P.-A. Baudat, F. Cerrina, P. Perfetti, B.P. Tonner, G. Margaritondo, Rev. Sci. Instrum. 69 (1998) 3106.
[23] T. Warwick, H. Ade, A.P. Hitchcock, H. Padmore, Ed.G. Rightor, B.P. Tonner, J. Electron. Spectrosc. Rel. Phenom. 84 (1997) 85.